A&A 390, 801–807 (2002)
DOI: 10.1051/0004-6361:20020740

Astronomy & Astrophysics

Optimum imaging observation wavelength selection for astronomical telescopes with partial correction adaptive optics

Changhui Rao and Wenhan Jiang

Adaptive Optics Laboratory, Institute of Optics and Electronics, Chinese Academy of Sciences, PO Box 350, Shuangliu, Chengdu 610209, Sichuan, PR China

Received 20 June 2001 / Accepted 15 April 2002

Abstract. In order to maximize the compensation potential of adaptive optics system for atmospheric turbulence, an appropriate observing wavelength should be selected on the basis of system capability and the working conditions to improve the optical resolution of astronomical telescopes. Based on the analysis of the wavefront residual error of the adaptive optics system, the optimum imaging observation wavelengths giving maximum imaging resolution of a partial correction adaptive optics system are derived for short-exposure and long exposure imaging respectively. The developed method is used to evaluate the optimum observing wavelength and the corresponding imaging resolution for the 61-element adaptive optical system at the 1.2 m telescope of the Yunnan Observatory.

Key words. telescopes – atmospheric effects – instrumentation: adaptive optics – methods: observational

1. Introduction

It is well known that atmospheric turbulence (Roddier 1981) severely limits the resolution of large ground-based telescopes in the visible and near infrared bands. Adaptive optics (Jiang et al. 1995) techniques can be used to correct random optical wavefront distortions induced by the atmospheric turbulence in real time.

The performance requirements for adaptive optics systems (AOS) depend on their mission. In the visible band, large telescopes require very complex AOS with hundreds of correction channels in order to produce high-resolution object images. But the large telescopes with low-order AOS perform well in the near infrared band. The imaging observation wavelength is one of the most significant factors in the requirements of AOS. For ground-based solar telescopes (Rimmele & Radick 1998), high-resolution monochromic imaging observations are usually done at a single wavelength with a very narrow band because of strong enough sunlight. For nighttime astronomical telescopes, a range of wavelengths is often used for imaging observation. For nighttime astronomical adaptive optical systems, the observing wavelength during setting up an observation is generally confined to the end portion of the red visible (R and I bands), the non-thermal near IR (J and H bands), or thermal IR (K band) according to the practical requirements and system capabilities.

In selecting an imaging observation wavelength, two competing effects must be considered. On the one hand, as the imaging wavelength is increased, the wavefront residual error decreases, resulting in a sharper point spread function. On the other hand, diffraction increases with wavelength, producing the opposite effect. For telescopes with partial correction AOS, the appropriate observing wavelength should be selected on the basis of the system capability and the working conditions in order to achieve the best angular resolution.

In previous publications, Tyler (Tyler & Fender 1994) derived an expression for the wavelength giving maximum resolution for the telescopes with AOS. In his study, the imaging Strehl ratio is simplified as $S = 1 - \sigma_{\rm fig}^2$, where $\sigma_{\rm fig}^2$ is the variance of the residual phase error. This is only valid for small residual phase error. For the partial correction AOS, this condition can commonly not be satisfied. In this paper, we derive the expressions of the optimum short-exposure and long-exposure imaging observation wavelength of astronomical telescopes with partial correction adaptive optics based on the analysis for the wavefront residual error of AOS. The paper is organized as follows. The parameters of atmospheric turbulence are briefly introduced in Sect. 2. In Sect. 3, the wavefront residual error of AOS is analyzed by considering the limitation factors of the practical AOS. Section 4 derives the optimum

Send offprint requests to: Changhui Rao,
e-mail: chrao@sc.homeway.com.cn

imaging observation wavelength on the basis of the relationship between the angular resolution and the wavefront residual error for the astronomical telescopes with partial correction AOS. In Sect. 5, the optimum imaging observation wavelength is computed for the 61-element adaptive optical system at the 1.2 m telescope of the Yunnan Observatory.

2. The parameters of atmospheric turbulence

The effects of atmospheric turbulence on astronomical telescopes are commonly characterized as the following atmospheric parameters: the turbulence coherence length, namely Fried's parameter r_0, the Greenwood frequency f_G, the Tyler frequency f_T, and the anisoplanatic angle θ_0. These parameters are usually specified at the visible wavelength of 0.55 μm (Roddier 1981):

$$r_0(\lambda_0) = \left[0.423k_0^2\, sec(\xi)\mu_0\right]^{-3/5}, \tag{1}$$

$$\theta_0(\lambda_0) = \left[2.91k_0^2\, sec^{8/3}(\xi)\mu_{5/3}\right]^{-3/5}, \tag{2}$$

$$f_G(\lambda_0) = 2.31\lambda_0^{-6/5}\, sec^{3/5}(\xi)\nu_{5/3}^{3/5}, \tag{3}$$

$$f_T(\lambda_0) = 0.368D^{-1/6}\lambda_0^{-1}\, sec^{1/2}(\xi)\nu_2^{1/2}, \tag{4}$$

where $k_0 = 2\pi/\lambda_0$ ($\lambda_0 = 0.55$ μm, $\mu_n = \int \mathrm{d}h C_n^2(h)h^n$, $\nu_n = \int \mathrm{d}h C_n^2(h)\nu^n(h)$. ξ is the zenith angle. $C_n^2(h)$ and $\nu(h)$ are the index-of-refractive model and wind speed profile respectively. Note that formula (4) is only effective for G-tilt, namely for an average gradient of the pupil.

3. Wavefront residual error for adaptive optics system

Most adaptive optics compensation systems apply the conjugate surface of the phase measured by WFS with a pair of active elements consisting of a high-speed TM and a DM. TM is usually used to correct the tilt component of the wavefront distortions induced by atmospheric turbulence. The figure (tilt-removed) component of the wavefront perturbation is compensated by DM. In the practical AOS, the compensation is not perfect because of the individual errors such as the uncompensated turbulence-induced error due to the finite bandwidth of the servo system and the measurement noise.

3.1. Figure residual error

The main figure residual errors include: (1) uncompensated turbulence-induced figure error due to the bandwidth of the figure compensation servo system; (2) closed-loop figure noise error due to the measurement error of the wavefront sensor; (3) fitting error due to the finite corrector elements; (4) anisoplanatic error due to the angular anisoplanatism and the focal anisoplanatism.

3.1.1. Uncompensated turbulence-induced figure error

The uncompensated turbulence-induced figure error depends on the temporal power spectrum of the figure (tilt-removed) component of the turbulence $F_{\mathrm{fig}}(f)$ and the servo control transfer function $H_c(jf)$:

$$\sigma^2_{\mathrm{fig\_tur}} = \int_0^\infty F_{\mathrm{fig}}(f)|1 - H_c(jf)|^2 \mathrm{d}f. \tag{5}$$

For Kolmogorov turbulence, the power spectrum of the figure (tilt-removed) component of the turbulence with the unit of rad^2/Hz, developed by Greenwood and Fried (Greenwood & Fried 1976), has the following form:

$$F_{\mathrm{fig}}(f) = \begin{cases} 0.132sec(\xi)k_0^2D^4\mu_0^{12/5}\nu_{5/3}^{-7/5}f^{4/3}, f \le 0.705D^{-1}\mu_0^{-3/5}\nu_{5/3}^{3/5} \\ 0.0326sec(\xi)k_0^2\nu_{5/3}f^{-8/3}, f \ge 0.705D^{-1}\mu_0^{-3/5}\nu_{5/3}^{3/5}. \end{cases} \tag{6}$$

In practical AOS, there exists a time delay between the wavefront sensing and wavefront correcting. Considering the effect of the time delay on servo control loop, the closed-loop transfer function of AOS can be expressed as (Rao et al. 2000)

$$H_c(jf) = \frac{e^{-j2\pi f\tau}}{1 + jf\Big/f_{3\mathrm{dB}}} \tag{7}$$

where $f_{3\mathrm{dB}}$ is the closed-loop -3dB bandwidth and τ is the time delay.

For high-bandwidth figure compensation, the uncompensated turbulence-induced figure error at the imaging wavelength λ can be obtained with the high-frequency form of the figure spectrum over the entire frequency range, so that (Li et al. 2000):

$$\begin{aligned} \sigma^2_{\mathrm{fig\_tur}} &\approx [f_G(\lambda)/f_{3\mathrm{dB}}]^{5/3}[1 + 2.2156(2\pi\tau f_{3\mathrm{dB}})^{2/3} \\ &\quad +1.3292(2\pi\tau f_{3\mathrm{dB}})^{5/3}] \\ &= (\lambda_0/\lambda)^2[f_G(\lambda_0)/f_{3\mathrm{dB}}]^{5/3}[1 + 2.2156(2\pi\tau f_{3\mathrm{dB}})^{2/3} \\ &\quad +1.3292(2\pi\tau f_{3\mathrm{dB}})^{5/3}]. \end{aligned} \tag{8}$$

3.1.2. Closed-loop figure noise error

In AOS, the noise resulting from WFS mainly consists of the photon shot noise due to the finite light intensity and the readout noise of the detector such as a CCD. Assuming the noise is white, the closed-loop figure noise error can be obtained as (Rao et al. 2000):

$$\begin{aligned} \sigma^2_{\mathrm{fig\_noise}} &= \int_0^{f_s/2} F_{\mathrm{fn}}|H_c(jf)|^2 \mathrm{d}f \\ &= F_{\mathrm{fn}} f_{3\mathrm{dB}}\, \mathrm{arctg}[f_s/(2f_{3\mathrm{dB}})] \end{aligned} \tag{9}$$

where F_{fn} is the noise power spectrum and f_s is the sampling frequency of the system.

Note that the wavefront measurement noise σ^2_{fn} relates the noise power spectrum to:

$$\sigma^2_{\mathrm{fn}} = F_{\mathrm{fn}} \cdot f_s/2. \tag{10}$$

Substituting Eq. (10) into Eq. (9), the closed-loop figure noise error at the imaging observation wavelength λ can be expressed as

$$\sigma^2_{\mathrm{fig\_noise}} = (\lambda_W/\lambda)^2\pi f_{3\mathrm{dB}}\sigma^2_{\mathrm{fn}}/f_s \tag{11}$$

where λ_W is the detecting wavelength of WFS and $\mathrm{arctg}[f_s/(2f_{3\mathrm{dB}})] \approx \pi/2$ is used.

3.1.3. Fitting error

The uncorrected phase error due to the figure (tilt-removed) component of turbulence at the imaging wavelength λ, namely figure fitting error, is conveniently expressed in terms of the ratio of the subaperture spacing and the turbulence coherence length (Hardy 1998):

$$\sigma^2_{\text{fig\_fit}} = 0.34[d_s/r_0(\lambda)]^{5/3} = 0.34(\lambda_0/\lambda)^2[d_s/r_0(\lambda_0)]^{5/3} \quad (12)$$

where d_s is the subaperture spacing.

3.1.4. Anisoplanatic error

When the beacon of AOS and the target object do not lie in the same direction, the error due to angular anisoplanatism at the imaging wavelength λ can be expressed as (Fried 1982)

$$\sigma^2_{\text{fig\_angle}} = (\theta/\theta_0(\lambda))^{5/3} = (\lambda_0/\lambda)^2(\theta/\theta_0(\lambda_0))^{5/3} \quad (13)$$

where θ is the angle between the beacon and the target object.

Furthermore, because the atmospheric turbulence is only partially detected by the beacon light, the use of laser beacons in AOS produces the error due to focal anisoplanatism, which may be expressed as (Tyler 1994)

$$\sigma^2_{\text{fig\_focus}} = (D/d_0(\lambda))^{5/3} = (\lambda_0/\lambda)^2(D/d_0(\lambda_0))^{5/3}, \quad (14)$$

where D is the diameter of the telescope. For the beacon with height H, the value of d_0 implied by Eq. (14) is

$$\begin{aligned} d_0(\lambda_0) &= \left\{k_0^2[0.057\mu_0^+(H) + 0.500\mu_{5/3}^-(H)/H^{5/3} \right. \\ &\quad \left. -0.452\mu_2^-(H)/H^2]\right\}^{-3/5}, \end{aligned} \quad (15)$$

where $\mu_m^+(H) = \int_H^\infty \mathrm{d}h\, sec^{m+1}(\xi)C_n^2(h)h^m$ and $\mu_m^-(H) = \int_0^H \mathrm{d}h\, sec^{m+1}(\xi)C_n^2(h)h^m$ and are the upper and lower turbulence moments at height H respectively.

3.1.5. Total figure residual error

The total figure residual error of AOS with the unit of phase rad^2 at the imaging wavelength λ may be expressed as the sum of individual errors in the form

$$\begin{aligned} \sigma^2_{\text{fig}} &= \sigma^2_{\text{fig\_tur}} + \sigma^2_{\text{fig\_noise}} + \sigma^2_{\text{fig\_fit}} + \sigma^2_{\text{fig\_anglet}} + \sigma^2_{\text{fig\_focus}} \\ &= (\lambda_0/\lambda)^2 \left\{[f_G(\lambda_0)/f_{3dB}]^{5/3}[1 + 2.2156(2\pi\tau f_{3dB})^{2/3} \right. \\ &\quad +1.3292(2\pi\tau f_{3dB})^{5/3}] \\ &\quad +(\lambda_W/\lambda_0)^2\pi f_{3dB}\sigma^2_{\text{fn}}/f_s + 0.34[d_s/r_0(\lambda_0)]^{5/3} \\ &\quad \left. +(\theta/\theta_0(\lambda_0))^{5/3} + (D/d_0(\lambda_0))^{5/3}\right\}. \end{aligned} \quad (16)$$

3.2. Tilt residual error

In AOS, the tilt component of turbulence is often measure by quadrant detectors and centroid trackers. This tilt belongs to G-tilt, namely average gradient over the pupil. The main errors involved in compensating the tilt component of turbulence are: (1) uncompensated turbulence-induced tilt error due to the bandwidth of the tilt compensation servo system; (2) closed-loop tilt noise error due to the measurement error of the tracking sensor.

According to the tracking frequency f_T defined by Tyler (Tyler 1994), see Eq. (4), the uncompensated turbulence-induced tilt error at the imaging wavelength λ can be expressed as

$$\sigma^2_{\text{tilt\_tur}} = [f_T(\lambda)/f_c]^2\,(\lambda/D)^2 = [f_T(\lambda_0)/f_c]^2\,(\lambda_0/D)^2 \quad (17)$$

where f_c is the closed-loop -3dB bandwidth of the tracking servo loop.

Similar to the closed-loop figure noise error, the closed-loop tilt noise error at the imaging wavelength λ relates the tilt measurement error σ^2_{tn}, the sampling frequency of the tracking system f_{st} and the closed-loop -3dB bandwidth of the tracking servo loop to

$$\sigma^2_{\text{tilt\_noise}} = (\lambda_T/D)^2\pi f_c\sigma^2_{\text{tn}}/f_{\text{st}} \quad (18)$$

where λ_T is the detecting wavelength of the tracking sensor. The tilt measurement error σ^2_{tn} is scaled as the unit of $(\lambda_T/D)^2$.

The total tilt residual error with the unit of tilt rad^2 at the imaging wavelength λ is given by the sum of the uncompensated turbulence-induced tilt error and the closed-loop tilt noise error,

$$\begin{aligned} \sigma^2_{\text{tilt}} &= \sigma^2_{\text{tilt\_tur}} + \sigma^2_{\text{tilt\_noise}} \\ &= (\lambda_0/D)^2\left\{[f_T(\lambda_0)/f_c]^2 + (\lambda_T/\lambda_0)^2\pi f_c\sigma^2_{\text{tn}}/f_{\text{st}}\right\}. \end{aligned} \quad (19)$$

4. Optimum imaging wavelength of the telescope with partial correction adaptive optics

The effect of wavefront residual error of AOS on an optical image is to remove energy from the central peak, distributing it into a surrounding halo. The halo is absent for a perfect wavefront, but dominates the image structure in the presence of a wavefront error typical of uncompensated turbulence.

For the astronomical telescope with AOS, the image resolution is most affected. To investigate the image quality of AOS, it is useful to begin with the extended Marechal approximation, which provides a relationship between the figure error and the Strehl ratio under weak-turbulence conditions

$$Strehl \approx \exp\left(-\sigma^2_{\text{fig}}\right). \quad (20)$$

This is only valid for small residual phase error. For most partial correction AOS, this condition is generally not satisfied.

Assuming all of the energy lost from the central core of the beam is scattered over a region of width $\lambda/r_0(\lambda)$, a composite short-exposure image Strehl ratio (Parenti & Sasiela 1994) for partial correction AOS can be shown as

$$Strehl_{\text{SE}} \approx \exp\left(-\sigma^2_{\text{fig}}\right) + \frac{1 - \exp\left(-\sigma^2_{\text{fig}}\right)}{1 + [D/r_0(\lambda)]^2}. \quad (21)$$

Accordingly, the short-exposure image resolution (Parenti & Sasiela 1994) for partial correction AOS can be expressed as

$$Resolution_{\text{SE}} \approx 1.22(\lambda/D)\left(1\Big/\sqrt{Strehl_{\text{SE}}}\right). \quad (22)$$

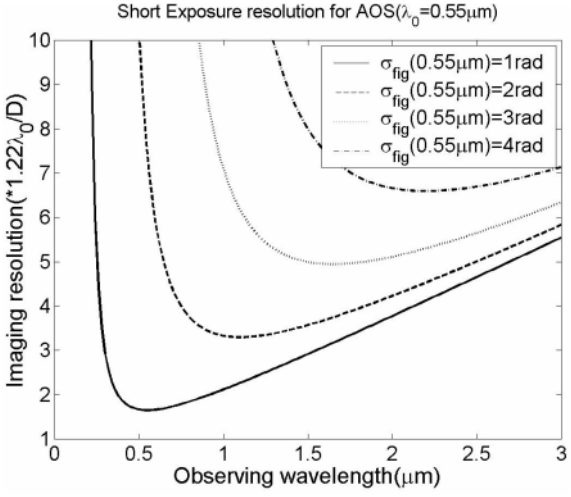

Fig. 1. The imaging resolution vs. observing wavelength for adaptive optical systems.

Similarly, for the long-exposure imaging, the Strehl ratio and the resolution (Parenti & Sasiela 1994) for AOS can be approximated to

$$Strehl_{\mathrm{LE}} \approx \frac{\exp\left(-\sigma_{\mathrm{fig}}^2\right)}{1+5(D/\lambda)^2\sigma_{\mathrm{tilt}}^2} + \frac{1-\exp\left(-\sigma_{\mathrm{fig}}^2\right)}{1+[D/r_0(\lambda)]^2} \tag{23}$$

and

$$Resolution_{\mathrm{LE}} \approx 1.22(\lambda/D)\left(1\Big/\sqrt{Strehl_{\mathrm{LE}}}\right) \tag{24}$$

respectively. Note that the first term of Eqs. (21) and (23) is the relative peak intensity of the central core of the imaging beam and the second term is that of the surrounding halo. Generally, the peak intensity of the central core is much larger than that of the halo for imaging with AOS. As the figure residual error is very small, the short-exposure Strehl ratio can be simplified as mentioned above. For partial correction adaptive optical systems, the imaging performance as shown in Eqs. (21–24) is by far superior.

Figure 1 presents the short-exposure imaging resolution of AOS versus the observing wavelength for different figure residual root mean square errors. It can be seen from Fig. 1 that for a certain figure residual error, the imaging resolution improves with increasing observing wavelength as the observing wavelength is relatively shorter. When the observing wavelength is longer, the imaging performance gradually becomes worse with the lengthening of the wavelength. Note that there exists an optimum observing wavelength in which the imaging resolution is highest for a certain figure residual error. The larger the figure residual error, the longer the optimum wavelength. So in astronomical telescopes with adaptive optics, the appropriate imaging observation wavelength need to be selected based on the system capability and its mission in order to exploit fully the compensation function of AOS for atmospheric turbulence.

The optimum wavelength would maximize the imaging resolution of the astronomical telescopes with adaptive optics. For convenience of analysis, a new function $F(\lambda)$ is defined to used to optimize the imaging observation wavelength of AOS,

$$F(\lambda) = (D/\lambda)^2 Strehl. \tag{25}$$

Evidently, the maximizations of the function $F(\lambda)$ and the imaging resolution are both equivalent.

4.1. Optimum wavelength for short-exposure imaging

For short-exposure imaging, the imaging resolution depends mainly on the figure residual error of AOS, so that $F(\lambda)$ can be written as

$$\begin{aligned} F(\lambda) &= (D/\lambda)^2 Strehl_{\mathrm{SE}} \\ &\approx (D/\lambda)^2\left[\exp\left(-\sigma_{\mathrm{fig}}^2\right) + \frac{1-\exp\left(-\sigma_{\mathrm{fig}}^2\right)}{1+(D/r_0(\lambda))^2}\right]. \end{aligned} \tag{26}$$

For astronomical imaging through adaptive optics correction for atmospheric turbulence, the imaging Strehl ratio and the resolution mostly lies on the intensity distribution of the central core of the beam. Note that generally the diameter of the system is much larger than the coherence length, namely $D \gg r_0(\lambda)$, so the function $F(\lambda)$ can be simplified as

$$F(\lambda) \approx (D/\lambda)^2 \exp\left(-\sigma_{\mathrm{fig}}^2\right). \tag{27}$$

Substituting Eqs. (16) into Eq. (27), one can obtain

$$F(\lambda) \approx (D/\lambda)^2 \exp[-A(\lambda_0/\lambda)^2] \tag{28}$$

where A is the figure residual error of AOS at the wavelength $\lambda_0 = 0.55\,\mu$m,

$$\begin{aligned} A &= [f_{\mathrm{G}}(\lambda_0)/f_{3\mathrm{dB}}]^{5/3}[1+2.2156(2\pi\tau f_{3\mathrm{dB}})^{2/3} \\ &\quad +1.3292(2\pi\tau f_{3\mathrm{dB}})^{5/3}] \\ &\quad +(\lambda_{\mathrm{W}}/\lambda_0)^2\pi f_{3\mathrm{dB}}\sigma_{\mathrm{fn}}^2/f_{\mathrm{s}} + 0.34[d_{\mathrm{s}}/r_0(\lambda_0)]^{5/3} \\ &\quad +(\theta/\theta_0(\lambda_0))^{5/3} + (D/d_0(\lambda_0))^{5/3}. \end{aligned} \tag{29}$$

In order to verify the existence of the optimum imaging observation wavelength, one can obtain, by taking the second order derivative for the function $F(\lambda)$ and letting it be less than zero, the following inequation:

$$\begin{aligned} \frac{\mathrm{d}^2F(\lambda)}{\mathrm{d}\lambda^2} &= \left(\frac{6D^2}{\lambda^4} - \frac{14AD^2\lambda_0^2}{\lambda^6} + \frac{4A^2D^2\lambda_0^4}{\lambda^8}\right) \\ &\quad \times\exp\left[-A(\lambda_0/\lambda)^2\right] < 0. \end{aligned} \tag{30}$$

Solving the above inequation, one can obtain

$$\sqrt{A/3}\lambda_0 < \lambda < \sqrt{2A}\lambda_0. \tag{31}$$

That is to say that there exists an optimum imaging observation wavelength for AOS only as $\sqrt{A/3}\lambda_0 < \lambda < \sqrt{2A}\lambda_0$.

Taking the first order derivative for the function $F(\lambda)$ and letting it be equal to zero, we can write:

$$\frac{\mathrm{d}F(\lambda)}{\mathrm{d}\lambda} = \left(\frac{-2D^2}{\lambda^3} + \frac{2AD^2\lambda_0^2}{\lambda^5}\right)\exp\left[-A(\lambda_0/\lambda)^2\right] = 0. \tag{32}$$

For short-exposure imaging, the optimum imaging observation wavelength for AOS, taking the solution of Eq. (32), can be derived as

$$\lambda_{\mathrm{SE\_opt}} = \sqrt{A}\lambda_0. \tag{33}$$

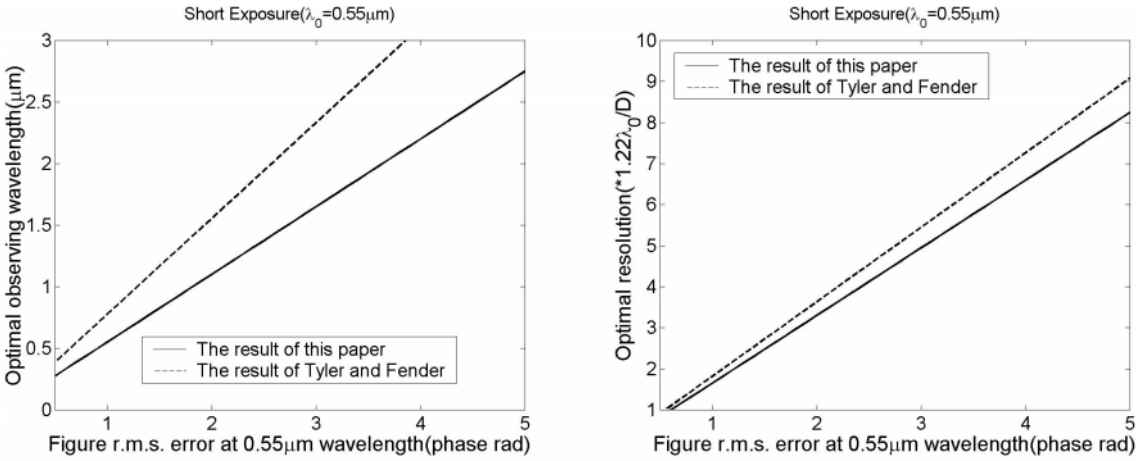

Fig. 2. Optimum short exposure observing wavelength and the corresponding image resolution.

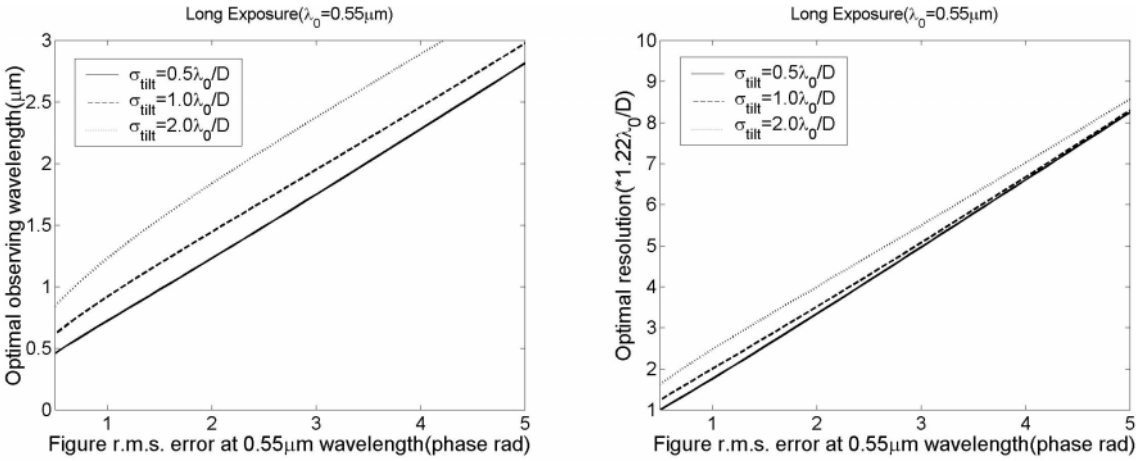

Fig. 3. Optimum long exposure observing wavelength and the corresponding image resolution.

According to Tyler (Tyler & Fender 1994), the optimal imaging observation wavelength for AOS should be

$$\lambda^*_{\mathrm{SE\_opt}} = \sqrt{2A}\lambda_0. \tag{34}$$

Subsituting Eq. (33) into Eq. (22), the corresponding resolution for short-exposure imaging at the optimum wavelength can be expressed approximately as

$$\begin{aligned} Resolution_{\mathrm{SE\_opt}} &\approx 1.22\sqrt{eA}(\lambda_0/D) \\ &= 1.22\sqrt{e}\left(\lambda_{\mathrm{SE\_opt}}/D\right). \end{aligned} \tag{35}$$

4.2. Optimum wavelength for long-exposure imaging

For long-exposure imaging, the imaging resolution depends not only on the figure residual error but also on the tilt residual error of AOS, Thus $F(\lambda)$ can be simplified as

$$F(\lambda) \approx (D/\lambda)^2 \frac{\exp[-A(\lambda_0/\lambda)^2]}{1 + 5B(\lambda_0/\lambda)^2} \tag{36}$$

where B is the tilt residual error of AOS at the wavelength $\lambda_0 = 0.55\ \mu$m,

$$B = [f_{\mathrm{T}}(\lambda_0)/f_{\mathrm{c}}]^2 + (\lambda_{\mathrm{T}}/\lambda_0)^2 \pi f_{\mathrm{c}} \sigma^2_{\mathrm{tn}}/f_{\mathrm{st}}. \tag{37}$$

Similarly, one can derive the optimum imaging observation wavelength for long-exposure imaging as

$$\lambda_{\mathrm{LE\_opt}} = \left[\sqrt{\left(A + \sqrt{A^2 + 20AB}\right)/2}\right]\lambda_0. \tag{38}$$

Subsituting Eq. (38) into Eq. (24), the corresponding resolution for long-exposure imaging at the optimum wavelength can be expressed approximately as

$$\begin{aligned} Resolution_{\mathrm{LE\_opt}} &\approx 1.22\left\{\left[\left(A + \sqrt{A^2 + 20AB}\right)/2 + 5B\right]\right. \\ &\quad \left.\times \exp\left[2\Big/\left(1 + \sqrt{1 + 20B/A}\right)\right]\right\}^{1/2}(\lambda_0/D) \\ &= 1.22\left\{\left[\left(A + \sqrt{A^2 + 20AB}\right) + 10B\right]\right. \\ &\quad \left.\times \frac{\exp\left[2\Big/\left(1 + \sqrt{1 + 20B/A}\right)\right]}{A + \sqrt{A^2 + 20AB}}\right\} \\ &\quad \times(\lambda_{\mathrm{LE\_opt}}/D). \end{aligned} \tag{39}$$

Figures 2 and 3 present optimum imaging observation wavelength and the corresponding image resolution for short-exposure imaging and long-exposure imaging respectively. It can be seen from Figs. 2 and 3 that the optimum imaging observation wavelength of AOS depends directly on the wavefront

residual error of AOS. The larger the wavefront residual error, the longer the optimum imaging observation wavelength is. Especially, the optimum imaging observation wavelength for short-exposure imaging, see Eq. (33), can be explained as the corresponding wavelength under the condition that the figure residual error is 1 rad^2.

Furthermore, the optimal observing wavelength and the corresponding short-exposure imaging resolution according to Tyler and Fender's (Tyler & Fender 1994) result, see Eq. (34), are also presented in Fig. 2. Note that the optimal wavelength derived by Tyler and Fender (Tyler & Fender 1994) is larger than that in this paper. The imaging performance according to Tyler and Fender's result is inferior to the result of this paper. The interpretation is that the imaging short-exposure Strehl ratio in Tyler and Fender's derivation (Tyler & Fender 1994) is approximated as $S = \exp(-\sigma_{\mathrm{fig}}^2) \approx 1 - \sigma_{\mathrm{fig}}^2$. If the required precision is 10%, the figure residual error should be less than 0.14 rad^2. When the figure residual error is equal to 0.6 rad^2, the precision can only attain 27%. In contrast with the results of this paper, the percentages of the departure of the optimal wavelength derived by Tyler and Fender (Tyler & Fender 1994) and the corresponding imaging resolution are 41.4% and 10% respectively. Evidently, the imaging resolution based on the calculated optimal observing wavelength in this paper is superior to that according to the optimal wavelength derived by Tyler and Fender (Tyler & Fender 1994). This result shows also that the calculation in this paper is more precise and more effective than the rough estimate carried by Tyler and Fender (Tyler & Fender 1994).

For nighttime astronomical telescopes with adaptive optics, the imaging observations are mostly done at a range of wavelengths. Figure 4 presents the percentage of the short-exposure imaging resolution departure from the optimum resolution as function of the percentage of the observing wavelength departure from the optimum wavelength. As AOS is not operated in the optimum wavelength but just 10% longer or shorter, the resolution degrades only about 1%. This result shows that the derived optimum observing wavelength in this paper can be applied not only in the monochromic observation with very narrow band but also in the nighttime observation with a certain range of wavelength.

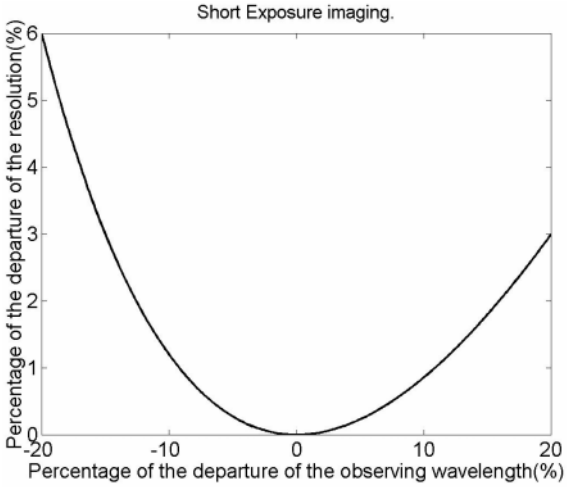

Fig. 4. The percentage of the short-exposure imaging resolution departure from the optimum resolution as a function of the percentage of the observing wavelength departure from the optimum wavelength.

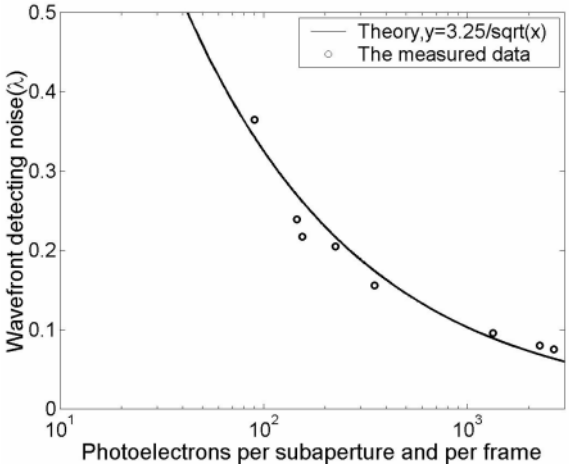

Fig. 5. The measured wavefront noise r.m.s. value vs. photoelectrons per subaperture and per frame.

5. Example

We have built a 61-element adaptive optical system at the 1.2 m telescope of the Yunnan Observatory (Jiang et al. 1998) for astronomical observations in the visible range. It consists of a 61-element deformable mirror, a Shack-Hartmann wavefront sensor with 8*8 subapertures and a digital wavefront processor. The detector of the Shack-Hartmann wavefront sensor is an intensified CCD with frame rate of 838 Hz. The effective diameter of the system is 1.06 m and the time delay is 2.8 T (T is the sampling period of the system). Figure 5 shows the experimental results of the measurement noise of WFS for the measured photoelectrons and its fitting curve. The measurement noise may be expressed as

$$\sigma_{\mathrm{fn}} = 3.25/\sqrt{P} \quad (\lambda_0) \tag{40}$$

where P is the photoelectrons detected by WFS per subaperture and per frame.

For this system, Fig. 6 presents the optimum short-exposure imaging observation wavelength and the corresponding image resolution as a function of the measured photoelectrons for the closed-loop bandwidth of 30 Hz, 60 Hz and 120 Hz respectively. During the computation, the anisoplanatic error is not considered and the following atmospheric parameters according to the statistial values at this site are taken: $r_0(\lambda_0)$ = 12.5 cm, $f_{\mathrm{G}}(\lambda_0)$ = 42 Hz.

It can be seen from Fig. 6 that for the reference beacon with high brightness, the larger the closed-loop bandwidth, the shorter the optimum imaging observation wavelength is, and the higher the corresponding resolution. For the reference beacon with low brightness, the reverse is true. This is due to the fact that the uncompensated turbulence-induced error, decreasing with the increasing closed-loop bandwidth, dominates over the total wavefront residual error in contrast with the closed-loop noise error, which is proportional to the closed-loop

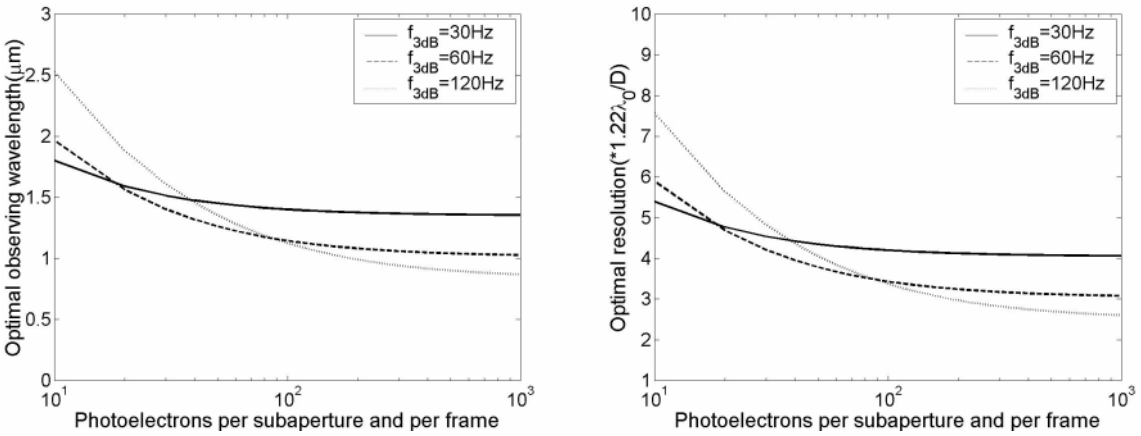

Fig. 6. Optimum observing wavelength and the corresponding image resolution as a function of photoelectrons per subaperture and per frame for different closed-loop bandwidths.

bandwidth, induced by the measurement error of the wavefront detector for the reference beacon with high brightness. For the reference beacon with low brightness, the closed-loop noise error is larger than the uncompensated turbulence-induced error. In this case, the wider the closed-loop bandwidth, the larger the total wavefront residual error.

6. Conclusion

In this paper, the figure residual error and the tilt residual error for adaptive optics systems are analyzed. The optimum imaging observation wavelengths giving the maximum resolution of a partial correction adaptive optics system are expressed as the function of the wavefront residual errors for short-exposure and long exposure imaging respectively. As an example, the optimum observing wavelength and the corresponding imaging resolution for the 61-element adaptive optical system at the 1.2 m telescope of the Yunnan Observatory are presented. The results show the optimum imaging observation wavelength of AOS depends directly on the wavefront residual error of AOS. The larger the wavefront residual error, the longer the optimum imaging observation wavelength.

Furthermore, it is necessary to note that the discrete nature of atmospheric transmission bands, the noise characteristics of the detector and its quatumn efficiency etc. must be considered for the selection of the practical imaging observation wavelength of astronomical telescopes with adaptive optics.

This work may be useful not only in designing adaptive optics system for astronomical telescopes but also in planning the experiments for astronomical telescopes with AOS.

Acknowledgements. This work is funded by the Hi-tech Project of China and National Natural Science Foudation of China (No. 19789301). The authors acknowledge the reviewers for valuable suggestions.

References

Fried, D. L. 1982, J. Opt. Soc. Am. 72, 52-61
Greenwood, D. P. 1976, J. Opt. Soc. Am. 66, 193-206
Hardy, J. W. 1998, Adaptive Optics for Astronomical Telescopes (New York, Oxford University Press)
Jiang, W., Li, M., Tang, G., et al. 1995, Opt. Eng., 34, 15-20
Jiang, W., Ling, N., Tang, G., et al. 1998, SPIE Proc., 3353, 696-703
Li, X., Jiang, W., Wang, C., & Xian, H. 2000, Acta Optica Sinica, 20, 10, 1328-1334
Parenti, R. R., & Sasiela, R. J. 1994, J. Opt. Soc. Am. A, 11, 288-309
Rao, C., Shen, F., & Jiang, W. 2000, Acta Optica Sinica, 20, 68-73
Rimmele, T. R., & Radick, R. R. 1998, SPIE Proceedings, 3353, 72-81
Roddier, F. 1981, The effects of atmospheric turbulence in optical astronomy, in Progress in Optics, ed. E. Wolf (North-Holland, Amsterdam), 19, 281-376
Tyler, D. W., & Fender, J. S. 1994, SPIE Proceedings, 2201, 227-238
Tyler, G. A. 1994, J. Opt. Soc. Am. A 11, 325-338
Tyler, G. A. 1994, J. Opt. Soc. Am. A 11, 358-367